Electronic Journal of Structural Engineering

Original Article

Cite this: DOI:10.56748/ejse.26897

Received Date: 09 October 2025
Accepted Date: 04 June 2026

1443-9255
https://ejsei.com/ejse

Optimization design of stability of coal mine roadway support structure based on improved GA-BP model

Yonghong Liu [a*], Zhengjun Zhao [b]

[a] Department of Resources and Security Engineering, Shanxi Engineering Vocational College, Taiyuan, 030009, China
[b] Taiyuan Coal Industry Design and Research Institute Group Co., Ltd
* Corresponding author: lyh437238@126.com

Abstract

To improve the stability of coal mine roadway support structures, Huainan Coal Mine was studied as the experimental object, and a Genetic Algorithm (GA) is proposed to optimize the Backpropagation (BP) neural network model. The global optimization and local prediction are coordinated through adaptive coding and other methods. GA is employed to optimize BP weights and thresholds to construct a loosening circle prediction model, and FLAC3D and orthogonal experiments are utilized to optimize support parameters. The experiment shows that the proposed GA-BP model has high accuracy in predicting loose circles. In the optimization of support parameters, the optimal combinations of support parameters for the development roadway, preparation roadway, and mining passage were determined, and the roof settlement under each working condition was controlled within the ideal range, resulting in significant support effects. The stability optimization design method for coal mine roadway support structure proposed in the study can accurately predict the extent of surrounding rock loosening zone and optimize support parameters, providing new ideas and methods for the stability design of deep roadway.

Keywords

Coal mine, Roadway, Support, GA-BP, Structure, Optimization, Orthogonal experiment

1. Introduction

As shallow coal resources are gradually depleted, mining operations are increasingly confronted with deep and intricate geological conditions, leading to frequent occurrences of events such as significant deformation of the surrounding rock (SR), floor heaving, and unstable support systems (Zhang et al., 2024). As the core of controlling the stability of the roadway, the design rationality of the support structure directly determines the engineering efficiency (Wu et al., 2023). However, traditional support design relies on empirical analogy, and the strength of support does not match the SR conditions, resulting in material waste and hidden safety hazards (Kianpour et al., 2024; Zhao et al., 2024). In recent years, some studies have attempted to introduce intelligent algorithms and numerical simulations for support optimization. Although genetic algorithms (GA) and neural networks have been introduced into geotechnical engineering, their prediction accuracy and generalization ability still need to be improved due to limitations such as fixed network structures, limited training samples, and single encoding methods. In addition, numerical simulations often use trial and error methods in optimizing support parameters, which makes it difficult to efficiently obtain the optimal combination (Yaghoubi et al., 2024). To conclude, this study proposes a GA-BP fusion model that uses GA to optimize the initial weights and thresholds of BP neural network, to improve the accuracy and stability of loose circle prediction, and inputs four indicators to predict the range of loose circles. Subsequently, by combining orthogonal experiments and FLAC3D numerical simulations, the influence of anchor parameters on roof displacement is systematically analyzed, achieving multi-objective optimization of support parameters. The research aims to optimize the range of rock loosening zones and support parameters, providing new ideas for the stability structure design of deep roadways. The innovation of this study lies in the following aspects: (1) The study constructed a loose circle range prediction model based on GA-optimized BP neural network to improve the accuracy and robustness of prediction. (2) By combining orthogonal experiments with FLAC3D numerical simulations, the influence of anchor rod length, diameter, spacing, and row spacing on roof displacement was systematically analyzed. (3) A method for optimizing tunnel support parameters by integrating intelligent prediction and numerical simulation was proposed, achieving scientific and precise support design.

2. Related Works

In recent years, the academic community has conducted multidimensional research, such as optimizing the bearing capacity of the bottom plate by combining steel bars and plain concrete strip arches or strengthening the stress transmission and energy compensation of the SR through ultra-high strength anchor rods (ARs) and high prestress support. Chen et al. proposed a zoning support method for irregular coal pillars by analyzing their failure characteristics and bearing mechanisms. This method divides the coal pillars into four zones: damaged, progressive, stable, and special. The method uses a combination support method of "pier pillar+flexible formwork concrete+grouting+high-strength anchor cable+U-shaped steel" for qualitative control. Monitoring data collected on-site indicated that the deformation and damage of newly excavated roadways were minimized after using this method, which could meet the requirements of safe and efficient engineering services (Chen et al., 2024). Pan et al. (2023) proposed an energy absorbing anti explosion support method based on disturbance response instability theory. This approach uses critical stress as an indicator to evaluate rock burst risk and establishes a prevention and control technology system through the coordinated control of stress reduction, disturbance reduction, weak physical properties, and energy absorbing support. The experimental outcomes revealed that the stability of the roadway was significantly improved after using this method, and effective suppression of rock burst disasters was achieved. Sun et al. (2023) proposed the combination technology of "presplitting and cutting top+constant resistance anchor cable", which is used for cutting top and releasing pressure in deep hole directional blasting, while using high prestress constant resistance anchor cable suspension. The on-site monitoring outcomes revealed that after using this technology, the stress of the SR decreased by 30%, the displacement decreased by 45%, and the stability of the roadway in the fault zone was significantly improved. Yao et al. (2023) proposed a combined support method of "36U steel+AR+anchor cable+full section grouting" to address the problem of easy damage to roadway anchoring structures under large dynamic pressure in short distances. This method first identifies the main cause of dynamic pressure deformation and then optimizes the support scheme through numerical simulation. The on-site monitoring outcomes revealed that after using the combination support scheme for 65 days, the convergence of the two sides was only 20 mm, the top plate settlement was 16 mm, the rock fissures were fully filled with grouting, and the stability of the roadway was significantly improved.

Babets et al. (2023) proposed a "numerical simulation+data grouping processing method algorithm" to optimize the parameters of roadway support for potential instability problems in longwall mining. This method uses Rocscience software coupled with the Hooke Brown criterion to simulate 81 combinations of coal thickness, SR strength, and width/strength of hardened mixture filling walls, and construct a top and bottom plate convergence prediction model. The experimental outcomes revealed that the shrinkage of the reserved roadway section was significantly reduced, and the stability was greatly improved. Huang et al. (2024) designed a composite reinforcement method for small coal pillars,

which includes "bi-directional pressure anchor cables, steel reinforced concrete piers, and advanced roof fractures," to solve the control problem of small coal pillar stability under mining disturbance in adjacent working faces. This reinforcement method first measures the disturbance threshold and overburden load and then sets up targeted support. The on-site monitoring outcomes revealed that the vertical deformation of the small coal pillar after using this method was 187mm, with a safety factor of 1.23, effectively suppressing dynamic pressure instability. Chen et al. (2023) proposed the method of "zone differentiation combined support" to address the issue of strong mining pressure under the remaining coal pillars in the nearby coal seam. This method divides the roadway under the coal pillar into zones A, B, and C according to their distance from the coal pillar. Zones A and C are secured in both directions with channel steel truss anchor cables, while zone B is supported by high resistance portal brackets. The experimental outcomes revealed that the deformation of the SR was within 210 mm after applying this method, and it could improve the safety of mining operations. Jiang et al. (2024) proposed the technology of confining lightweight concrete roof and rib support structure for attaining steady management overSR in self-formed roadways. This technology initiates by constructing a mechanical model for roof support, subsequently deducing the computational formula for the combined forces acting on the roof support structure. It further elucidates how the parameters of the self-formed roadway impact the forces within the roof support framework. The experimental outcomes revealed that this approach could effectively improve the stability of goaf without coal pillars.

In summary, although the above research has achieved significant results in roadway support, most still rely on empirical analogy or single factor optimization, lacking intelligent prediction of the range of rock loosening zones and systematic coordination of support parameters. The existing methods have failed to effectively integrate intelligent algorithms with numerical simulations, resulting in significant deficiencies in prediction accuracy and parameter optimization efficiency in support design. In response to the aforementioned research gaps, this study proposes a GA-BP fusion model that combines orthogonal experiments and FLAC3D numerical simulations to achieve accurate prediction of the loosening zone range and multi-objective optimization of support parameters, providing new ideas for the stability design of deep tunnels.

3. Methods and materials

3.1 Classification and detection methods of SR

Loose zone is an unstable area formed after roadway excavation due to stress redistribution and changes in rock mechanics properties (Liu et al., 2024; Ma et al., 2024). The loose zone is a fractured zone formed by the impact of mining on the SR of the roadway. The smaller its range, the better the stability of the SR. More reliable support methods need to be adopted to increase support strength or optimize support structures. At this time, the SR is more prone to deformation and damage, and the supporting structure needs to withstand greater pressure and deformation, with higher reliability requirements. The research mainly uses geological radar detection as the main method, while also utilizing borehole observation instruments for detection. The uniaxial compressive strength of rock refers to the maximum compressive stress at which a rock specimen reaches failure under uniaxial pressure, and its calculation formula is shown in equation (1).

$$\sigma = \frac{F}{A} \tag{1}$$

In equation (1), F represents the maximum axial load at the time of specimen failure, measured in N. A represents the cross-sectional area of the specimen, measured in m^2. The Brazilian splitting test serves as an indirect approach for assessing the tensile strength of rocks and is applicable to disc-shaped rock specimens (Liu et al., 2023). The study also uses the SUNS 890 series electro-hydraulic servo dynamic fatigue testing machine for Brazilian splitting tests, and the detailed calculation procedure is presented in equation (2).

$$\sigma_t = \frac{2P}{\pi Dt} \tag{2}$$

In equation (2), P represents the maximum load at which the specimen fails, measured in N. D is the diameter of the specimen, measured in m. t is the thickness of the specimen, measured in m. In the variable angle shear test, the rock specimen is placed in a shear fixture and the shear characteristics of the rock in different directions are studied by changing the shear angle. For a given shear angle, the normal stress and shear stress on the failure surface of the specimen can be calculated. Assuming that the axial stress σ of the specimen during the loading process is known, the normal stress σ_n and the shear stress τ can be calculated based on the shear angle θ. The calculation formulas for the two are presented in equation (3).

$$\begin{cases} \sigma_n = \sigma\cos^2\theta \\ \tau = \sigma\sin\theta\cos\theta \end{cases} \tag{3}$$

In equation (3), θ represents the shear angle, which is the angle between the shear plane and the axis of the specimen. Due to the comprehensive influence of multiple factors on the range of rock loosening zone, to clarify the main influencing factors to support the selection of prediction indicators, this study is based on previous research, statistics of relevant literature, and analysis of its influencing factors using SPSS software. The study first selects 16 influencing factors to form a set, coded them according to the SPSS sample requirements, and then imports the data into the software to establish a database. The coding results of each factor are presented in Fig. 1.

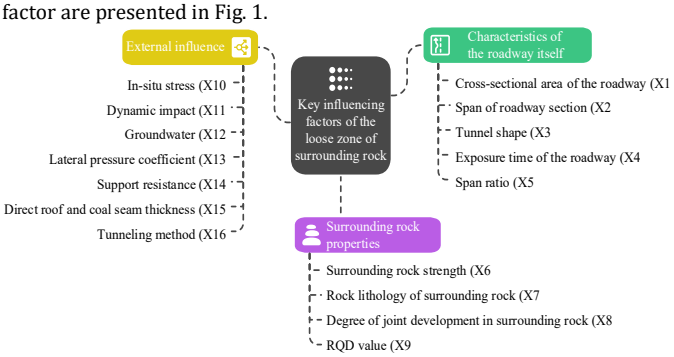

Fig. 1 Factor coding results

In Fig. 1, the characteristics of the roadway itself reflect the influence of roadway structure and existence status on the loosening zone from dimensions such as spatial size and exposure duration. The properties of SR reflect its own physical and mechanical properties, such as strength, integrity, etc., and are the basic conditions for determining the loosening zone. External factors include geological stress environment, mining disturbance, water action, support and construction methods, and other external intervention factors. These factors can change the stress and deformation environment of the SR, thereby affecting the range of the loosening zone.

3.2 GA-BP model construction and training methods

The loose zone is formed by the combined action of rock strength and stress, with rock strength being the main influencing factor and uniaxial compressive strength as the indicator. The geostress is related to the depth of the roadway and is an important influencing factor. The span of the roadway affects the redistribution of stress in the loose zone, and the degree of joint development in the SR weakens the strength of the rock, promoting the development of the loose zone. Preliminary consideration is given to four factors, including the strength of SR and the ground stress, among others. There is a functional relationship between the rebound value of rock mass and the uniaxial compressive strength, which has been effectively used in related engineering to predict this strength (Khajevand, 2023; Rahman & Sarkar, 2023). Based on the feasibility and convenience of on-site acquisition, four indicators including rebound value, roadway burial depth, joint development degree, and roadway span will be used as prediction indicators for the loosening zone, and quantification is planned. The calculation formula for rock rebound value R is shown in equation (4).

$$\sigma_u = a \times R^b \tag{4}$$

In equation (4), R represents the rebound value. a and b are fitting parameters and need to be determined based on actual test data. The burial depth of a roadway refers to the vertical distance from the roof of the roadway to the surface, measured in meters. The degree of joint development refers to the distribution density, scale, connectivity, and impact on the integrity of the rock mass. It is mainly evaluated through quantitative indicators such as joint spacing, joint number, and joint density. In the rock mass quality index method, the degree of joint development is usually divided into undeveloped (joint spacing greater than 1m), slightly developed (joint spacing 0.5-1m), moderately developed (joint spacing 0.2-0.5m), and developed (joint spacing less than 0.2m). The auxiliary evaluation is carried out through quantitative indicators, and the specific calculation formula is shown in equation (5).

$$\begin{cases} J = \frac{L}{N} \\ D = \frac{N}{S} \end{cases} \tag{5}$$

In equation (5), J is the spacing between joints. L represents the total length of the measurement section, measured in m. N represents the number of joint strips within the measurement section. D indicates the density of joints. S is the measurement area, measured in m^2. Currently, obtaining the range of the loose circle mainly relies on on-site measurement or mathematical model prediction. Measurement requires carrying heavy equipment, a large workload, and is easily affected by harsh environments and instrument failures, resulting in high costs. BP networks are easily affected by initial weights and thresholds during training. Improper initial values can lead to slow convergence, divergence,

or oscillation, and poor stability, making it difficult to meet practical prediction needs (Zhu et al., 2023). GA mimics the genetic evolution process of organisms to identify the optimal solution, enabling it to optimize the weights and thresholds within BP neural networks. To improve the accuracy of predicting the loosening zone of SR, a BP neural network optimized by GA is studied to accelerate convergence speed, improve prediction performance and calculation accuracy. Fig. 2 shows the steps of the GA-BP algorithm.

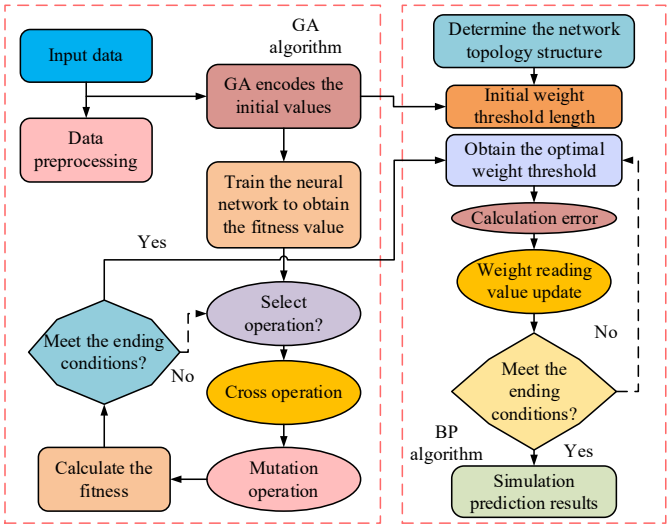

Fig. 2 GA-BP algorithm steps

In Fig. 2, the process of the GA-BP algorithm begins with input data and training data. Through GA, the weights and thresholds to be optimized in the BP neural network are encoded to generate an initial population. Subsequently, the fitness of individuals is calculated to evaluate their performance, and selection operations are carried out based on fitness to filter out high-quality individuals. Then, through crossover and mutation operations, which simulate biological evolution, a new population is generated. This iterative optimization continues until the termination conditions of the GA are met, at which point the optimized weights and thresholds are output. Following this, the process moves to the neural network phase. The network is constructed and initialized using optimized parameters. Input data are then used for training, and the error between predicted and actual values is calculated. Based on this error, the weights and thresholds are updated through BP. Iteration continues until the training termination conditions of the neural network are satisfied, after which the output results are utilized for prediction. The termination condition is usually that the error converges to the preset accuracy, the error no longer decreases after multiple consecutive iterations or reaches the maximum number of iterations. This study sets the error convergence accuracy to 0.01 (mean square error), the maximum number of iterations to 100, and uses an early stopping mechanism to terminate training when the error no longer decreases after 5 consecutive iterations. The structure of the GA-BP loose circle prediction model developed in this study is shown in Fig. 3.

In Fig. 3, the model inputs four indicators of the influence of the loose circle and outputs the range of the loose circle. The input layer has four nodes, and the output layer has one node. It adopts a single hidden layer structure with nine hidden layer nodes. The model processes data input through activation functions. GA optimizes network weights to improve the global search ability of the model, while BP neural network performs local optimization through gradient descent to adjust weights to minimize prediction errors.

3.3 Optimization design method for support parameters

In roadway engineering, different geological conditions require different support strategies. By optimizing support parameters, the stability of the roadway can be enhanced and the occurrence of safety accidents such as collapse can be reduced. If chosen improperly, high strength will cause material waste, increase costs, and slow down excavation speed due to complex construction. Insufficient strength makes it impossible to control the deformation of the SR, which may readily result in safety accidents such as roof collapse. Therefore, optimizing support methods and parameters is essential. Orthogonal experiments can be conducted on the SR types of Huainan coal mine, and orthogonal design combined with numerical analysis methods can be used to optimize and analyze the spray anchor support scheme. An appropriate constitutive model is selected based on the physical and mechanical properties of the SR. The level of orthogonal experimental factors and simulation scheme design are shown in Table 1.

Table 1. Orthogonal Experimental Factor Levels and Simulation Scheme Design

Experiment Number	AR length (m)	AR diameter (mm)	AR spacing (m)	AR row spacing
1	1.6	16.0	1.0	1.2
2	1.8	18.0	1.2	1.2
3	1.6	18.0	1.0	1.0
4	1.8	16.0	1.2	1.2
5	1.8	18.0	1.1	1.0
6	1.8	20.0	1.0	1.0

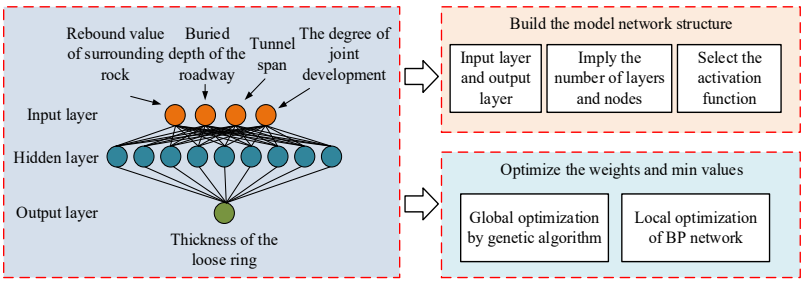

Fig. 3 The loosening circle prediction model based on GA-BP

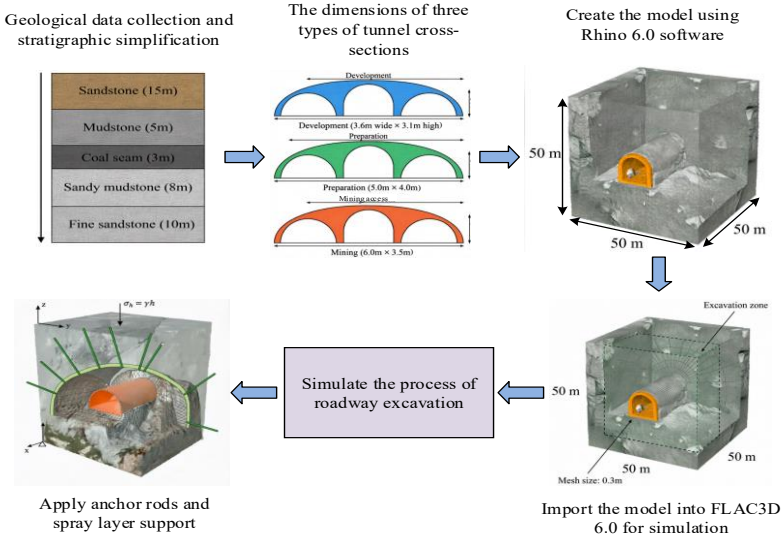

Fig. 4 Construction process of geological model

Based on the six sets of support parameter combinations in Table 1, a FLAC3D geological model is established to extract the displacement of the top plate under different combinations of anchor bolt parameters and record the maximum settlement value of the top plate for each set of experiments, in order to determine the optimal combination of support parameters. The construction process of the geological model is illustrated on Fig. 4.

In Fig. 4, the SR of Huainan Coal Mine is mainly Class III, with thick rock blocks, so the model is entirely enclosed in a single lithological block. A 50m×50m×50m mining field model with different roadways is built using Rhino 6.0, the grid is divided and imported into FLAC3D 6.0. The roadway includes development (3.6m×3.1m), preparation (5.0m×4.0m), and mining access (6.0m×3.5m), all of which are three arch structures. When simulating excavation and support in FLAC3D, the SR model is first built, the grid is partitioned, and material properties are assigned. Excavation is carried out step by step, with support added after each step: the Cable element is employed to simulate anchor bolts, with their properties and segment configurations set accordingly; the Shell element is used to simulate shotcrete layers, with parameters defined and connections to the SR ensured. Boundary conditions and initial stresses are applied, and equilibrium calculations are performed to ensure a reasonable initial state. Finally, the model is solved to analyze the deformation and stress of the SR as well as the forces acting on the support, thereby evaluating its effectiveness. After the geological model is established, boundary conditions need to be set lateral and bottom displacements are restricted on all surfaces except the top surface. The top surface serves as a free displacement boundary, where the self-weight stress of the overlying rock mass, which exhibits a linear relationship with the burial depth, is applied. The calculation is shown in equation (6).

$$\sigma_h = \gamma h \tag{6}$$

In equation (6), γ represents the bulk density of the rock layer, measured in kg/m³. h is the buried depth of rock stratum, measured in m. Mohr-Coulomb criterion is a commonly used yield criterion in rock mechanics and soil mechanics, which is used to describe the failure behavior of materials under shear stress (Chechekhina et al., 2024). Under three-dimensional stress conditions, the Mohr-Coulomb criterion can be expressed as equation (7).

$$f = \sigma_1 - \sigma_3 - 2c\cos\phi - (\sigma_1 + \sigma_3)\sin\phi \leq 0 \tag{7}$$

In equation (7), σ_1 represents the max principal stress. σ_3 is the min principal stress. ϕ represents the internal friction angle. c indicates cohesion. When $f = 0$, the material reaches a yielding state. When $f > 0$, the material is damaged. Optimizing support parameters for different types of roadways is an important step in ensuring roadway stability, safety, and economy. In numerical simulation, hexahedral elements are used for the mesh, with a mesh density of 0.5 m × 0.5 m × 0.5 m (densified to 0.2 m within 2 m around the roadway). The constitutive model adopts the Mohr-Coulomb model, with a bulk density of 25 kN/m³, an elastic modulus of 2.5 GPa, a Poisson's ratio of 0.25, a cohesive force of 1.2 MPa, an internal friction angle of 32 °, and a tensile strength of 0.8 MPa.

4. Results

4.1 Verification of loose ring prediction model based on GA-BP

Huainan Coal Mine is one of the important coal production bases in China, located in the central northern part of Anhui Province, with geographical coordinates of approximately 116° 21′ -117° 12′ E longitude and 32° 25′ -33° 00′ N latitude. The total mining area is about 3000 square kilometers, and a multi-level (middle section) development system is adopted. The current mining level is concentrated between -500m and -1000m, and each level is divided into panels or mining areas, using comprehensive mechanized coal mining technology. The diameter of the development roadway is 6-8m, and the preparation roadway is 4.5-5.5m wide and 3.5-4.5m high. The mining roadway is 4.0-4.5m wide and 3.0-3.5m high. To test the predictive ability of the GA-BP model, test samples were used to simulate and predict through the trained model. The research compared the true value with the predicted value. If the error met the standard, the model was better. Otherwise, tuning and retraining were required. Experimental conditions and parameter configurations are presented in Table 2.

In MATLAB, the training process of neural networks typically involved iteratively optimizing the network using sample data to minimize training errors. During the training process, the neural network adjusted its weights and biases based on the input sample data to gradually reduce errors. The iteration and training error curves are presented in Fig. 5.

Table 2. Experimental conditions and parameter configurations

Device name	Model/Specification	Parameter category	Numerical value
MATLAB software	Version 2020a	Training function	trainlm
Geological radar	RIS-K2 of IDS Company, Italy	Number of iterations	30
Borehole viewer	Wuhan Tianchen Weiye ZKXG30	Cross probability	0.8
Rebound instrument	BT-225 Mechanical rebound tester	Mutation probability	0.2
SUNS 890 series electro-hydraulic servo machine	Shenzhen Sunstest Technology Co., LTD.	Learning rate	0.01

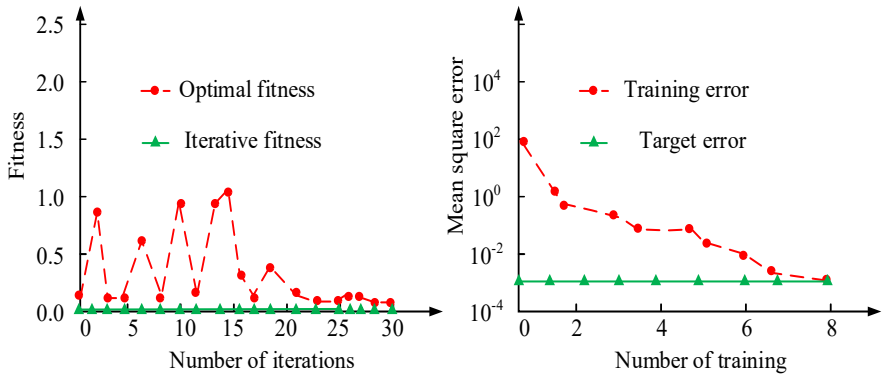

(a) The iterative process of the GA (b) Model training error curve

Fig. 5 Iteration and training error curve

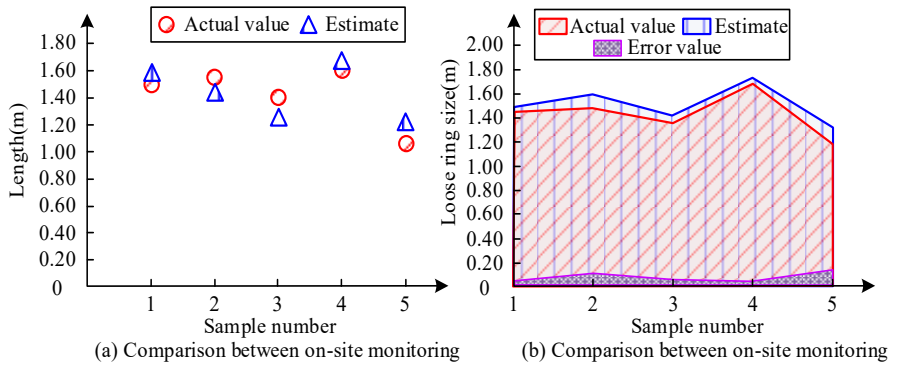

(a) Comparison between on-site monitoring results and model calculation values (b) Comparison between on-site monitoring results of loose ring and model calculation values

Fig. 6 Prediction ability of the model based on predicted value and actual value

From Fig. 5(a), during the initial iterations, both the optimal fitness and the worst fitness were close to 0. As the iteration count increased, the optimal fitness gradually rose, reaching approximately 1.5 at the 10th iteration, about 2.5 at the 20th iteration, and ultimately approximately 4.5 at the 30th iteration. The worst fitness exhibited significant fluctuations in the first 10 iterations but gradually stabilized thereafter, ultimately approaching 0 at the 30th iteration. This indicates that the GA gradually optimized during the iterative process, with fitness values continuously improving. From Fig. 5(b), it is evident that as the training epoch count increased, the mean squared error (MSE) of the model gradually decreased. When the training epoch count was 0, the MSE was approximately 0.045; it dropped to about 0.025 after 1 training epoch, continued to decline to around 0.015 after 5 training epochs, and ultimately reached its lowest point of approximately 0.01 after 8 training epochs. This demonstrates that the model's performance gradually improved during the training process, with errors continuously decreasing and the model's prediction accuracy steadily enhancing. To evaluate the model's predictive capability, normalization was applied to the input layer of five sets of test data. The trained model was then called for prediction, followed by inverse normalization of the outputs. The model's predictive capability was assessed by comparing the predicted values with the actual values, with the results shown in Fig. 6.

The comparison between the measured and predicted values of the five samples in Fig. 6 (a) shows a significant difference in the accuracy of the model prediction. Among them, sample 4 had an error of 1.13cm, accounting for 0.6%, with the highest accuracy. Sample 5 had an error of 13.64cm, accounting for 12.5%, with the largest error. The errors of the remaining samples ranged from 1.14cm to 15.22cm. The actual values fluctuated between samples 1 and 5, with a maximum of 1.65m and a minimum of 1.09m. As shown in Fig. 6 (b), the predicted values of the loose circle were close to the actual values, but there was a deviation. The maximum error of 0.15m was reached in sample 3, and the minimum error was close to 0m. Overall, the fluctuation of the loose circle did not affect the support design, and the predicted value was close to the actual value with a small error, indicating that the prediction model had high accuracy.

4.2 Experimental analysis of support parameter optimization

The SR of Huainan coal mine is mainly classified as Class III (moderately stable), especially in deep high stress areas, belonging to the middle loose zone. Orthogonal experiments could reduce the number of experiments and had the same effect. The simulation results of the orthogonal experiment on Class III SR in the development roadway are presented in Fig. 7.

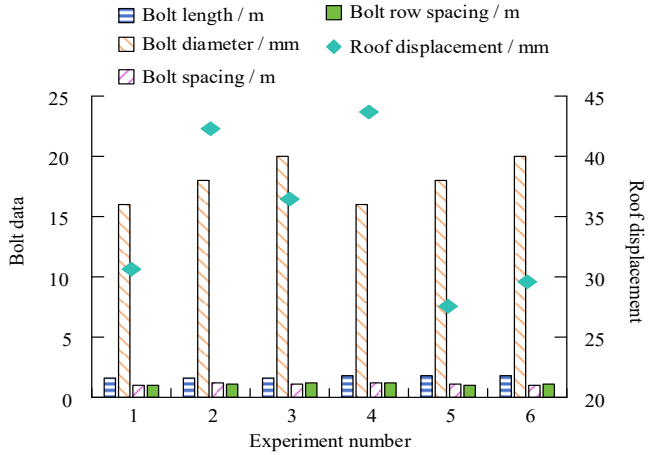

Fig. 7 Simulation results of orthogonal experiments on rock mass class Ⅲ in roadways

According to Fig. 7, in the experiment, the length of the ARs was divided into two levels: 1.6m and 1.8m, the diameter was divided into three levels: 16mm, 18mm, and 20mm, and the spacing and row spacing of the ARs were divided into two levels: 1.0m and 1.2m. The experimental outcomes revealed that the displacement of the top plate varied between 27.56mm and 43.68mm. Among them, Experiment 4 had the largest displacement of the roof, reaching 43.68mm, corresponding to AR parameters of 1.8m, 16mm diameter, 1.2m spacing, and 1.2m row spacing. The displacement of the top plate in Experiment 5 was the smallest, at 27.56mm, corresponding to anchor parameters of 1.8m, 18mm diameter, 1.1m spacing, and 1.0m row spacing. The intuitive relationship of Class III SR in the development roadway is presented in Fig. 8.

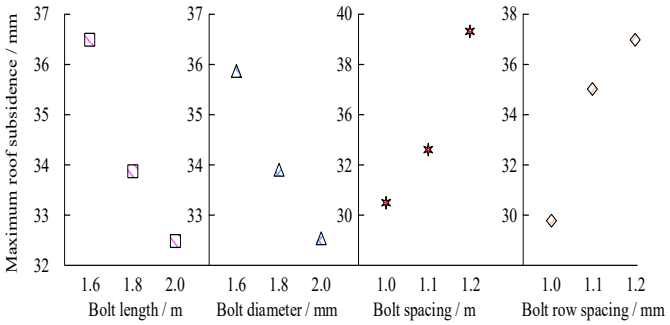

Fig. 8 The intuitive relationship between roadway and class Ⅲ SR

According to Fig. 8, as the AR length increased from 0.6m to 2.0m, the width of the SR below the AR length decreased from 40mm to 25mm, indicating that as the AR length increased, the width of the SR gradually decreased. In the AR diameter diagram, as the diameter increased from 0.6m to 2.0m, the width of the SR below the AR diameter decreased from 40mm to 25mm, indicating that the larger the AR diameter, the smaller the width of the SR. In the anchor spacing diagram, the spacing increased from 0.6m to 1.2m, and the width of the SR below the anchor spacing increased from 20mm to 40mm, indicating that as the anchor spacing increased, the width of the SR also increased. In the AR spacing diagram, the spacing increased from 0.6m to 1.2m, and the width of the SR below the AR spacing increased from 20mm to 40mm, indicating that as the AR spacing increased, the width of the SR also increased. Overall, it can be concluded that Plan 5 had the smallest maximum subsidence of the roof and the best support effect. Therefore, its AR parameters were used as support parameters for Class III SR development roadways. The orthogonal experimental simulation results of Class III SR in the preparation roadway are presented in Fig. 9.

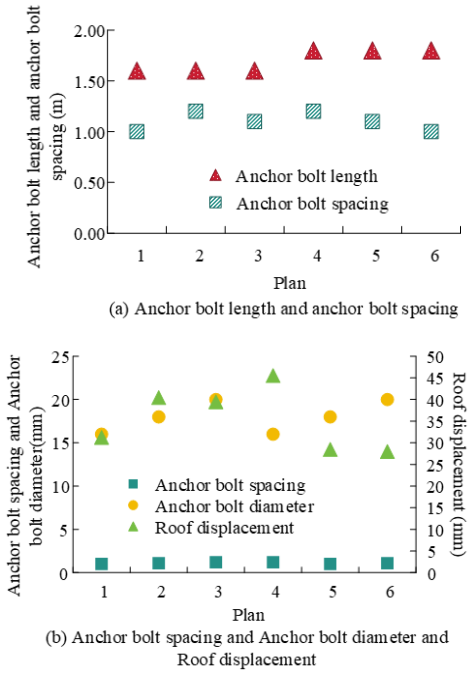

Fig. 9 Simulation results of orthogonal experiments on class Ⅲ SR in preparation roadway

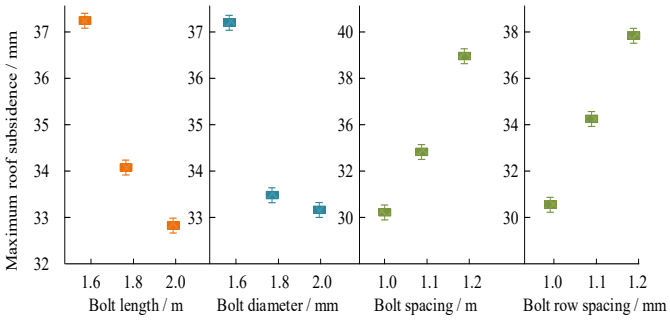

Fig. 10 The intuitive relationship between preparation roadway and class Ⅲ SR

According to Fig. 9, in experiments 1 to 4, the length of the AR increased from 1.6m to 1.8m, the diameter increased from 16mm to 20mm, the spacing and row spacing increased from 1.0m to 1.2m, and the

displacement of the roof increased from 31.25mm to 45.53mm. The length of the AR in experiments 5 and 6 was 1.8m, the diameter was 18mm and 20mm, the spacing and row spacing were 1.1m and 1.0m, and 1.0m and 1.1m, respectively, and the displacement of the roof was 28.47mm and 27.98mm, respectively. The intuitive relationship between the preparation of Class III SR in the roadway is shown in Fig. 10.

Fig. 10 shows that when the length of the AR ranged from 1.6m to 2.0m, the maximum subsidence of the roof decreased from 37mm to 32mm, indicating that increasing the length of the AR helped to reduce subsidence. The diameter of the AR increased from 16mm to 20mm, and the maximum subsidence of the roof decreased from 37mm to 33mm, indicating that increasing the diameter could also reduce subsidence. As the spacing and row spacing increased from 1.0m to 1.2m, the maximum subsidence of the roof increased from 30mm to 39mm, indicating that an increase in spacing and row spacing would lead to an increase in subsidence. These data indicated that increasing the length and diameter of ARs helped to reduce roof subsidence, while increasing spacing and row spacing was the opposite. Overall, it can be concluded that Plan 6 had the smallest maximum subsidence of the roof and the best support effect. Therefore, its AR parameters were used as the support parameters for the preparation roadway of Class III SR. The orthogonal experimental simulation results of Class III SR in mining access are presented in Fig. 11.

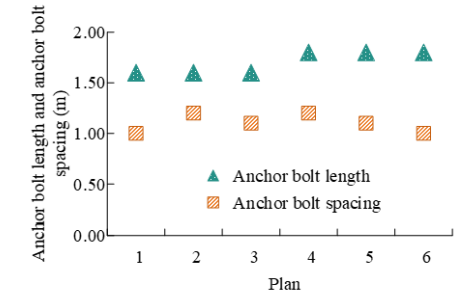

(a) Anchor bolt length and anchor bolt spacing

(b) Anchor bolt spacing and Anchor bolt diameter and Roof displacement

Fig. 11 Simulation results of orthogonal experiments on rock mass of Class III in mining roadway

According to Fig. 11, in experiments numbered 1 to 6, the length of the AR varied between 1.6m and 1.8m, while the diameter of the AR varied between 16mm and 20mm. The spacing and row spacing of ARs varied between 1.0 and 1.2m. There were significant differences in the displacement of the roof under different experimental conditions, with Experiment No. 4 having the largest displacement of 48.63mm, while Experiment No. 5 had the smallest displacement of only 29.44mm. The intuitive relationship between Class III SR in mining access is shown on Fig. 12.

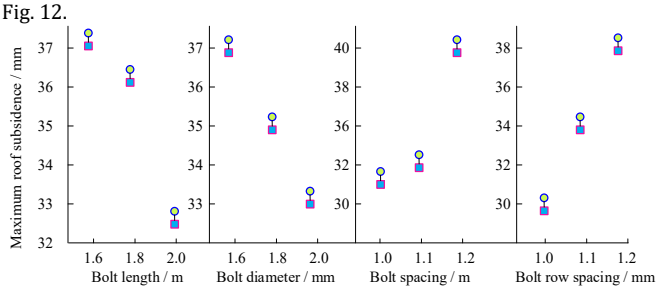

Fig. 12 The intuitive relationship between mining approach and class III SR

Fig. 12 shows that as the AR length increased from 1.6m to 2.0m, the max roof subsidence decreased from 37mm to 32mm. The AR diameter increased from 16mm to 20mm, and the max roof subsidence decreased from 37mm to 33mm. The AR spacing increased from 1.0m to 1.2m, and the max roof subsidence increased from 30mm to 41mm. The AR spacing increased from 1.0m to 1.2m, and the max roof subsidence increased from 30mm to 39mm. These data revealed that increasing the AR length and diameter helped to reduce the max roof subsidence, while increasing the AR spacing and spacing led to an increase in the max roof subsidence. Overall, it can be concluded that Plan 5 had the smallest max subsidence on the roof and the best support effect. Therefore, its AR parameters were used as the parameters for the mining access of Class III SR.

5. Discussion and Conclusion

To improve the scientificity of roadway support structure design, reduce material waste and safety hazards caused by traditional support design methods, this study optimized the initial weights and thresholds of BP neural network through GA. Meanwhile, FLAC3D numerical simulation software was employed to optimize the support parameters of different types of roadways in Huainan Coal Mine. Orthogonal experiments were conducted to analyze the influence of factors such as AR length, diameter, spacing, and row spacing on the max subsidence of the roadway roof, and to determine the optimal combination of support parameters.

The results indicated that the GA-BP model had high accuracy in predicting the range of rock loosening zones. In the test samples of Huainan coal mine, the max error between the model predicted value and the actual value was 13.64cm, accounting for 12.5% of the error, while the min error was only 1.13cm, accounting for 0.6% of the error. Overall, the predicted values were close to the actual values with small errors, indicating that the model could effectively predict the range of loose circles. In terms of optimizing support parameters, increasing the length and diameter of ARs helped to reduce the max subsidence of the roof, while increasing the spacing and row spacing of ARs led to an increase in subsidence. In the orthogonal experiment of developing Class III SR in the roadway, Scheme 5 had the smallest max subsidence of the roof, only 27.56mm, corresponding to anchor parameters of 1.8m length, 18mm diameter, 1.1m spacing, and 1.0m row spacing. In the experiment of preparing roadway and mining access, Scheme 6 and Scheme 5 were determined as the optimal combination of support parameters, with max roof subsidence of 27.98mm and 29.44mm, respectively, showing good support effects. The GA-BP model proposed in this study combined the global search capability of GA algorithm with the local approximation advantage of BP neural network, effectively solving the problems of traditional BP network being prone to getting stuck in local optima and slow convergence speed. It showed high accuracy and stability in predicting the range of loose circles. This method only required four easily obtainable indicators on site, namely rebound value, burial depth, joint development degree, and tunnel span. It had strong engineering practicality and promotion value and can be applied to the design of coal mine tunnels, transportation tunnels, and underground engineering support under similar geological conditions.

However, the sample data used in this study were mainly from Huainan Coal Mine, and the geological conditions were relatively simple. The generalization ability of the model in other mining areas needs to be verified. In addition, the input indicators only considered four main factors and did not take into account dynamic influences such as geostress and water action. Therefore, in future research, the sample collection scope should be further expanded to cover multiple mining areas and lithological conditions, in order to enhance the generalization ability of the model. Meanwhile, algorithms such as particle swarm optimization or Bayesian optimization are introduced to automatically optimize network hyperparameters, and multiple factors such as groundwater and geostress fields are considered to be included in the prediction system to further improve the accuracy and applicability of the model.

Fundings

The research is supported by Shanxi Engineering Vocational College's 2024 College level Project "Research and Implementation Plan for Hydraulic Fracturing Technology in Mining Face" (HX-2024113).

References

Babets, D., Sdvyzhkova, O., Hapieiev, S., Shashenko, O., & Prykhodchenko, V. (2023). Multifactorial analysis of a gateroad stability at goaf interface during longwall coal mining-A case study. Mining of Mineral Deposits, 17(2), 9-19. https://doi.org/10.33271/mining17.02.009

Chechekhina, E., Voloshin, N., Kulebyakin, K., & Tyurin-Kuzmin, P. (2024). Code-Free machine learning solutions for microscopy image processing: Deep learning. Tissue Engineering Part A, 30(19-20), 627-639. https://doi.org/10.1089/ten.tea.2024.0014

Chen, D., Wang, X., Zhang, F., Bai, J., Zhao, X., Li, M., Yu, Y., Wang, X., & Sun, S. (2024). Study on the mechanism of progressive instability of special-shaped coal pillar and the stability control of roadway under the influence of mining. Rock Mechanics and Rock Engineering, 57(8), 6461-6483. https://doi.org/10.1007/s00603-024-03798-6

Chen, D., Ma, X., Wu, Y., Xie, S., Li, H., Jiang, Z., Wang, E., Guo, F., Guo, W., & Ye, Q. (2023). Failure mechanism and divisional differentiated control of surrounding rock in mining roadway under remaining coal pillar in close-

distance coal seam. Energy Science & Engineering, 11(4), 1412-1435. https://doi.org/10.1002/ese3.1400

Huang, W., Zhao, T., Zhang, C., Liu, Y., Sui, L., Hou, T., & Jiang, D. (2024). Assessment of pillar stability and its control in a double roadway layout. Energy Science & Engineering, 12(10), 4192-4209. https://doi.org/10.1002/ese3.1884

Jiang, B., Wang, M. Z., Wang, Q., Xin, Z. X., Xing, X. Y., Deng, Y. S., & Yao, L. D. (2024). Bearing mechanism of roof and rib support structure in automatically formed roadway and its support design method. Journal of Central South University, 31(7), 2467-2487. https://doi.org/10.1007/s11771-024-5678-4

Khajevand, R. (2023). Prediction of the uniaxial compressive strength of rocks by soft computing approaches. Geotechnical and Geological Engineering, 41(6), 3549-3574. https://doi.org/10.1007/s10706-023-02473-x

Kianpour, M., & Raza, S. (2024). More than malware: unmasking the hidden risk of cybersecurity regulations. International Cybersecurity Law Review, 5(1), 169-212. https://doi.org/10.1365/s43439-024-00111-7

Liu, H., Jing, H., Yin, Q., Zhao, Z., Meng, Y., & Zhang, L. (2023). Study on mechanical properties and fracture behavior of granite after thermal treatment under Brazilian splitting test. KSCE Journal of Civil Engineering, 27(2),643-656. https://doi.org/10.1007/s12205-022-0296-x

Liu, R., Jiang, D., He, Y., Zhang, H., Chen, J., Ren, S., & Zhou, Z. (2024). Study on cooling measures and ventilation cooling device of high ground temperature tunnel. Journal of Thermal Analysis and Calorimetry, 149(8), 3347-3365. https://doi.org/10.1007/s10973-024-12910-5

Ma, K., Zhang, J., Zhang, J., Feng, J., Zhou, P., & Kong, C. (2024). Determination of the rock mass bearing mechanism following excavation of circular tunnels. Rock Mechanics and Rock Engineering, 57(8), 5783-5800. https://doi.org/10.1007/s00603-024-03840-7

Pan, Y., & Wang, A. (2023). Disturbance response instability theory of rock bursts in coal mines and its application. Geohazard Mechanics, 1(1), 1-17. https://doi.org/10.1016/j.ghm.2022.12.002

Rahman, T., & Sarkar, K. (2023). Empirical correlations between uniaxial compressive strength and density on the basis of lithology: implications from statistical and machine learning assessments. Earth Science Informatics, 16(2), 1389-1403. https://doi.org/10.1007/s12145-023-00969-x

Sun, X., Wang, J., Zhang, Y., Zhao, W., Guo, Z., He, M., Chen, F., & Miao, C. Y. (2023). Stability control measures for roof cutting and NPR supporting mining roadways in fault areas of kilometre-deep coal mine. Journal of Mountain Science, 20(10), 3051-3065. https://doi.org/10.1007/s11629-023-8152-0

Wu, Z., Zhao, Y., & Zhang, N. (2023). A literature survey of green and low-carbon economics using natural experiment approaches in top field journal. Green and Low-Carbon Economy, 1(1), 2-14. https://doi.org/10.1002/gj.4937

Yaghoubi, E., Yaghoubi, E., Khamees, A., & Vakili, A. H. (2024). A systematic review and meta-analysis of artificial neural network, machine learning, deep learning, and ensemble learning approaches in field of geotechnical engineering. Neural Computing and Applications, 36(21), 12655-12699. https://doi.org/10.1007/s00521-024-09893-7

Yao, W., Liu, G., Pang, J., & Huang, X. (2023). Instability mechanism and surrounding rock control technology of roadway subjected to mining dynamic loading with short distance: A case study of the Gubei Coal Mine in China. Geotechnical and Geological Engineering, 41(2), 1407-1427. https://doi.org/10.1007/s10706-022-02343-y

Zhang, W., Tang, X., Yang, W., Jiang, J., Zhang, H., & Li, P. (2024). Review of tunnels and tunnelling under unfavourable geological conditions. Geological Journal, 59(9), 2668-2689. https://doi.org/10.1002/gj.4937

Zhao, L., Fan, X., Hawbani, A., Xu, L., Yu, K., Liu, Z., & Alfarraj, O. (2024). Generative abnormal data detection for enhancing cellular vehicle-to-everything-based road safety. IEEE Transactions on Green Communications and Networking, 8(4), 1466-1478. https://doi.org/10.1109/TGCN.2024.3400403

Zhu, J., Zheng, H., Yang, L., Li, S., Sun, L., & Geng, J. (2023). Evaluation of deep coal and gas outburst based on RS-GA-BP. Natural Hazards, 115(3), 2531-2551. https://doi.org/10.1007/s11069-022-05652-w

Disclaimer